Tensor Networks and Quantum Error Correction

Andrew J. Ferris[1,2,3] and David Poulin[3]
[1]ICFO—Institut de Ciencies Fotoniques, Parc Mediterrani de la Tecnologia, 08860 Barcelona, Spain
[2]Max-Planck-Institut für Quantenoptik, Hans-Kopfermann-Strasse, 1, 85748 Garching, Germany
[3]Département de Physique, Université de Sherbrooke, Québec J1K 2R1, Canada
(Received 30 January 2014; published 16 July 2014)

We establish several relations between quantum error correction (QEC) and tensor network (TN) methods of quantum many-body physics. We exhibit correspondences between well-known families of QEC codes and TNs, and demonstrate a formal equivalence between decoding a QEC code and contracting a TN. We build on this equivalence to propose a new family of quantum codes and decoding algorithms that generalize and improve upon quantum polar codes and successive cancellation decoding in a natural way.

DOI: 10.1103/PhysRevLett.113.030501 PACS numbers: 03.67.Pp, 02.70.-c, 03.67.Hk, 89.75.Hc

The basic principle of quantum error correction (QEC) is to encode information into the long-range correlations of entangled quantum many-body states in such a way that it cannot be accessed locally. When a local error affects the system, it leaves a detectable imprint—called the error syndrome. The decoding problem consists in inferring the recovery with greatest probability of success given the error syndrome. In general, this is a hard problem [1,2], but for well-chosen codes, it can be solved efficiently either exactly (e.g., [3,4]) or heuristically (e.g., [5,6]).

Entangled many-body states generally have a number of parameters that increase exponentially with the number of particles, and so are not amenable to direct numerical calculations. Tensor network (TN) states were introduced [7–9] as families of many-body states that are specified with only polynomially many parameters. In this setting, the evaluation of physical quantities of interest such as correlation functions and local expectation values reduces to contracting the indices of a TN. In general, the contraction of a TN is a difficult problem [10], but some TNs can be efficiently contracted [7,9,11,12], sometimes using heuristic approximations [8,13].

In this Letter, we explore and deepen the relation between QEC and TNs and leverage this relationship to propose new encoding and decoding techniques. First, we establish a formal connection between the decoding problem for QEC and TN contraction. We then describe the correspondence between a number of well known TN families and QEC codes. Finally, we exploit this equivalence to propose a new family of efficiently decodable QEC codes that naturally generalize quantum polar codes [14–20] based on a recently introduced family of TNs called branching MERA [21]. We study their performance numerically and find that they outperform polar codes. Further, our numerics clearly demonstrate good code performance is possible without using entanglement assistance. In a companion paper [22], we present a detailed study of the classical analogue of these new codes.

Quantum error correction—In general, a $[[n, k, d]]$ quantum code $\mathcal{C}$ is a 2^k-dimensional subspace of an n-qubit Hilbert space. The integer d is the minimum distance of the code, and indicates the number of simultaneous errors that it can correct. The code can be defined as the image of a unitary encoding circuit U acting on an n-qubit state, where k "data qubits" can be in an arbitrary state and the other $n-k$ "syndrome qubits" are restricted to the state $|0\rangle$,

$$\mathcal{C} = \{|\psi\rangle = U|\phi\rangle_k \otimes |0\rangle^{\otimes n-k} : |\phi\rangle_k \in (\mathbb{C}^2)^{\otimes k}\}. \quad (1)$$

Subjected to an error E, the encoded state $|\psi\rangle$ is transformed to $|\psi'\rangle = E|\psi\rangle$. Measuring the syndrome qubits on the state $U^\dagger|\psi'\rangle$ yields the error syndrome, and the decoding problem consists in identifying the optimal recovery given the syndrome. In this Letter, we define quantum codes in terms of their encoding circuit U.

Decoding as TN contraction—We now explain how the decoding problem can be expressed as a TN contraction. We focus on Clifford encoding circuits and Pauli channels; the general case is treated in the Supplemental Material [23]. Recall that the n-qubit Pauli group consists of tensor products of the four Pauli matrices I, σ_x, σ_y, and σ_z and that Clifford circuits map that group to itself.

Pauli channel noise models assign probabilities $P_n(E = E_1 \otimes E_2 \otimes \ldots \otimes E_n) = P(E_1)P(E_2)\ldots P(E_n)$ to each element E of the Pauli group, where $P(E_i)$ is a probability distribution. Hence, P is represented by a rank-one tensor of dimension 4, that is $P = (p_I, p_x, p_y, p_z)$. Consider the distribution $Q_n(E) = P_n(U^{-1}EU)$ corresponding to the distribution of errors after the de-encoding circuit U^{-1}. This distribution is obtained by contracting the encoding circuit (viewed as a rank $2n$ tensor) with the P's, as in Fig. 1(a). To decode, we condition this probability distribution on the observed error syndrome, and typically decode one qubit at a time for efficiency reasons.

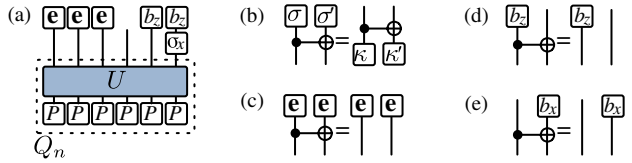

FIG. 1 (color online). (a) General decoding problem. This TN encodes the probability distribution $Q_4(E|s)$ of qubit 4 given that the 5th and 6th qubits revealed the syndrome $s = (0, 1)$. (b)–(e) Action of the CNOT gate on the bimodal indicator functions. The truth table for (b) $(\sigma, \sigma') \to (\kappa, \kappa')$ is given by $(I, \sigma_x) \to (I, \sigma_x)$, $(\sigma_x, I) \to (\sigma_x, \sigma_x)$, $(I, \sigma_z) \to (\sigma_z, \sigma_z)$, and $(\sigma_z, I) \to (\sigma_z, I)$. Identities (c)–(e) follow from the application of (b) to bimodal indicator functions.

Prior to encoding, the syndrome qubits were in state $|0\rangle$, as in Eq. (1). After de-encoding, these qubits are measured in the basis σ_z to reveal the error syndrome (the ± 1 outcomes are usually denoted $\{0, 1\}$). A syndrome 0 doesn't strictly imply an error-free qubit. Instead, it indicates that it either had no error or a σ_z error—providing no information about the z quadrature. Thus, the probability tensor representing such a measurement outcome is a bimodal indicator function on I and σ_z, i.e., $b_z = (1, 0, 0, 1)$. Similarly, a syndrome 1 is consistent with either a σ_x or a σ_y error, corresponding to the bimodal indicator function $\bar{b}_z = (0, 1, 1, 0)$. Note that $\bar{b}_z = \sigma_x b_z$. Thus, conditioning the distribution $Q_n(E)$ on the syndrome is achieved by contracting it with b_z or $\bar{b}_z$. To trace out a qubit from the distribution, we simply contract Q_n with the uniform distribution $\mathbf{e} = (1, 1, 1, 1)$ on that qubit. Figure 1(a) illustrates the resulting TN. Later, to efficiently contract the TNs corresponding to the polar and branching-MERA codes, we will make use of circuit identities shown at Figs. 1(b)–(e). There, we also must prepare and measure qubits in the other quadrature. We use the bimodal indicator function $b_x = (1, 1, 0, 0)$ in the case where a syndrome qubit prepared in the $|+\rangle$ state and later measured along σ_x.

We exhibit relations between well-studied QEC codes and TNs below:

Convolutional codes.—These codes are defined by the "staircase" quantum circuit represented at Fig. 2(a) [24,25]. Given unentangled input data, the resulting encoded state will have rather limited entanglement, as entanglement between each step is mediated by only a constant number of "memory" qubits. As a consequence, these codes have a constant minimal distance. The corresponding states define matrix product states (MPS) [26], which accurately describe the ground state of gapped one-dimensional quantum systems, and are the variational class of states behind density matrix renormalization group [27].

It is possible to exactly evaluate the error probability of each data qubit using a message passing algorithm [5]. This problem and corresponding method are formally equivalent to the transfer-operator method used to compute local expectation values from a MPS [26]. In QEC, it is also possible to determine the globally optimal recovery using Viterbi's algorithm [4]. Similar techniques have been proposed to determine the optimal MPS approximation to a ground state [28].

Turbo codes.—Turbo codes are constructed from the interleaved concatenation of convolutional codes, where the interleaver consists of a random permutation of the qubits between the two encoding circuits [5]. This leads to long-range entanglement, and therefore larger minimum distances. The decoding procedure is analogous to an approximation used in many-body physics to solve two spin chains that are coupled by random, nonlocal interactions. In those terms, the transfer operator is used to evaluate local expectation values in each chain and the nonlocal interchain interactions are treated by mean field.

Concatenated block codes.—These are defined by the tree-shaped quantum circuit of Fig. 2(b). Their importance stems from their role in fault tolerance [29]. Tree TNs underlie some early real-space renormalization methods for quantum systems [30], and continue to be used more recently [11,31–33]. The contractibility of this TN has led to an exact (maximum likelihood) decoding algorithm for concatenated codes [3] offering significant improvements over conventional (minimum distance) decoders.

Topological codes.—Such codes correspond to the degenerate ground space of a local, gapped two-dimensional Hamiltonian, which include model systems for topological order such as Kitaev's quantum double [34] and Levin-Wen string-nets [35]. These systems can be described by projected entangled pair states (PEPS) [36], a family of TN that are a natural generalization of MPS to higher

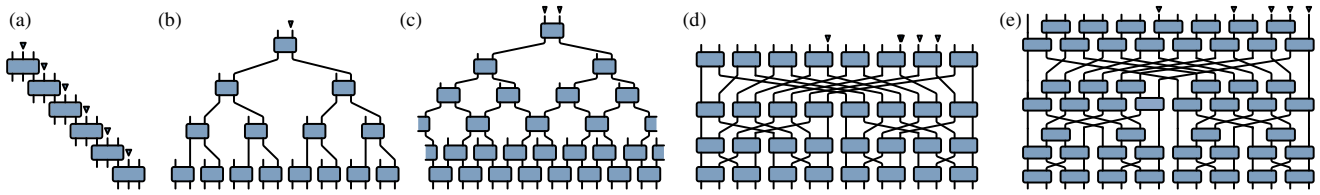

FIG. 2 (color online). Graphical definitions of various unitary TNs and encoding circuits of QEC codes: wires represent one or a few qubits, rectangles represent unitary transformation with time running from top to bottom. The size of each circuit can be varied in an obvious way. For coding applications, location of the data qubits are indicated by triangles, other qubits are initialized to $|0\rangle$ (or $|+\rangle$). (a) MPS TN and convolutional codes. (b) Tree TN and concatenated quantum block codes. (c) MERA TN and topological code. (d) Branching tree TN and polar codes. (e) Branching MERA TN and codes introduced in this Letter.

dimensions [8]. PEPS are generally not efficiently contractable, and consequently there exists no efficient, exact decoding algorithm for topological codes. Heuristic renormalization group methods have been devised both in the context of PEPS contraction [13] and topological code decoding [6], and in both case can offer accurate estimates.

Topological codes can also be represented by a different family of TN—the multiscale entanglement renormalization ansatz (MERA) [37], defined at Fig. 2(c). These TNs accurately describe the ground states of critical one dimensional systems [9], as well as some two dimensional systems, including exact descriptions of some with topological order [37]. MERA can be accurately contracted for the evaluation of k-point correlation function, but the complexity scales exponentially with k. Unfortunately, in this case the decoding problem is formally equivalent to the evaluation of an n-point correlation function, so the correspondence with MERA does not yield an efficient decoding method for topological codes.

Polar codes.—The spectral (or branching tree) tensor network of Fig. 2(d) has a structure identical to the fast Fourier transform and thus is useful for representing highly entangled states of (noninteracting) fermions [38]. Arikan's polar code and its generalizations can be defined by that circuit, where every gate is a CNOT. The exact location of the data qubits depend on the noise model and the rate of the code. Determining the optimal location of the data qubits (ignoring any correlations between decoding errors) is realized by Arikan's so-called "genie decoder" [39], and can be formulated as a tensor contraction problem. Decoding is realized using Arikan's successive cancellation decoder which similarly can be recast as a TN contraction as we will explain below. Because they obey a special self-duality condition, polar codes can be used to encode quantum information [15,16], where in general they can attain the coherent information rate [17,19].

Branching MERA codes.—The spectral TN can be seen as a simplification of branching MERA shown on Fig. 2(e), where half of the gates (sometimes called the disentanglers) have been removed. Branching MERA states were introduced in physics as a variational class of efficiently-contractible TN states with large amounts of entanglement [12]. While the amount of entanglement between a block of length L and the rest of the chain is bounded by a constant in MPS and by $\log L$ in MERA and tree TN, it can be as large as L in a branching MERA, the maximum allowed by quantum mechanics.

We define branching MERA codes as the (classical or quantum) code resulting from the family of encoding circuit illustrated Fig. 2(e), with all gates CNOTs, and with the location of data qubits depending on the channel and encoding rate. (Note that, unlike the tree and MERA codes mentioned earlier, the orientation of this unitary circuit is reversed compared to their usual orientation in many-body physics, making the contractions efficient). One small difference in the quantum setting is that not all input stabilizer qubits are set to the state $|0\rangle$; some are set to $|+\rangle$. The choice of which input qubit carries data, which are set to $|0\rangle$ and which are set to $|+\rangle$ is a problem called channel selection which will be addressed below. Before, we explain how decoding is done.

Decoding polar and branching MERA codes.—We first adapt Arikan's successive cancellation decoder to the quantum setting by decoding the two quadratures (x and z errors) in succession. First, x errors are decoded sweeping from right to left. Assume that all qubits to the right of position i have a fixed bimodal distribution b_z or $\bar{b}_z$, either because they were z-type syndrome qubits or because we have already determined if they have undergone x-type error. The idea of successive cancellation is to determine the value of x-type errors on qubit i conditioned on this information only, ignoring any information about qubits to the left of position i, which are thus contracted with $\mathbf{e}$. The resulting TN for branching MERA is therefore represented by Fig. 3(a). Using the circuit identities of Fig. 1, this TN is equivalent to Fig. 3(b), which has a tree-width 3 (meaning that the intermediate steps of the decoder need only deal with distributions over at most 3 qubits), and can therefore be efficiently contracted [with cost $\mathcal{O}(n)$]. Afterwards, z-type errors are decoded in a similar fashion, sweeping

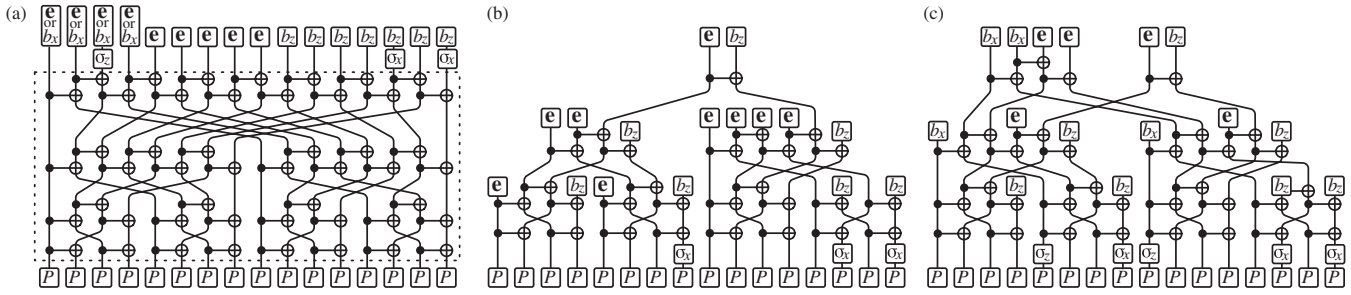

FIG. 3. Tensor network representation of the branching MERA code. (a) This TN encodes the x error probability of the seventh qubit (from right) knowing that among the first six qubits, only the first and third had x errors, among the last four qubits, only qubit 14 had a z error, and ignoring everything about qubits 8 to 12. The decoder can choose to ignore the information about x errors, in which case the four tensors b_x on the left are replaced by $\mathbf{e}$. Using the circuit identities of Fig. 1, these two TNs for z decoder and the symmetric x-z decoder become equivalent to (b) and (c).

from left to right reducing the bimodal distributions b_z and $\bar{b}_z$ to a single Pauli channel $(I, \sigma_x, \sigma_y, \sigma_z)$. When taking care to recycle previous calculations, the total decoding procedure has numerical cost $\mathcal{O}(n \log n)$. Decoding of polar codes follows straightforwardly since they are obtained by removing gates from branching MERA circuits.

We have also implemented a symmetric decoder where x- and z-type errors are decoded simultaneously, sweeping from the right for x errors and from the left for z errors. This can provide an advantage because x and z errors are typically correlated. On a depolarization channel for instance, where $p_x = p_y = p_z$, this correlation is mediated by y errors which are seen as a combination of x and z errors (remember $\sigma_z\sigma_x = i\sigma_y$). Thus, knowing about z errors at the time of decoding x errors provides additional information which enhances the decoding performance. As shown at Fig. 3(c), the resulting TN has tree width equal to 6 for branching-MERA (or 2 for polar codes), so this decoding scheme is also efficient.

To understand the origin of this contractibility, and hence the efficiency of the two decoders described above, note that the circuit identities can be used to remove all CNOTs in the encoding circuit Fig. 3(a) when all top tensors are identical (either all $\mathbf{e}$, b_x, b_z or I). Thus, the complexity comes from "domain walls" between different kinds of distributions. Contracting a TN with one or two domain walls is equivalent to computing a one- or two-point correlation of a branching MERA, which can be done efficiently [21].

Numerical results.—We now numerically investigate the performance of these codes and decoding techniques for the depolarizing channel (further results, including for the erasure channel, are in the Supplemental Material [23]).

The first stage of the procedure is to select which logical channels will carry quantum information and which will be fixed in either the x or z basis. The performance of a single quadrature of a given logical channel can be characterized independently from the remainder with Monte Carlo sampling techniques. In this procedure, we determine the probability that a given decision (i.e., determining an error in either the x or z basis) is incorrect assuming all the prior decisions were correct. As in [20], we then select the data channels to be those with the lowest error rate on the worst quadrature (and fixing the remaining qubits in the x and z basis depending on which quadrature performs worse). See the Supplemental Material [23] for a detailed study of channel polarization.

In Fig. 4(a), we plot the performance of the polar code (with standard decoder), the polar code with symmetric decoder and the branching-MERA code (with standard decoder) as a function of depolarization probability. In all cases we see a relatively sharp crossover between a low-error rate regime and a high-error rate regime, occurring somewhat below the depolarizing rate 9.92% where the coherent information and code rates coincide. We observe

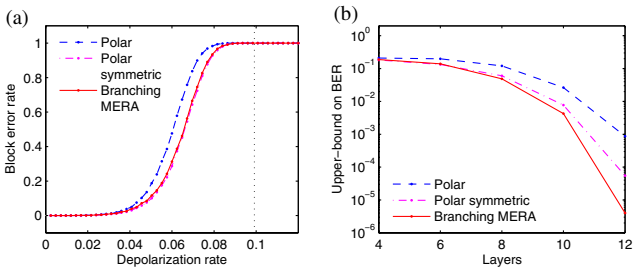

FIG. 4 (color online). Performance of the polar and branching-MERA codes under the depolarizing channel. The block-error rate (BER) is the probability of incorrectly decoding a block on n qubits. (a) Comparison of the various codes and decoding algorithms for codes of size 2^{12} qubits with encoding rate $1/2$. (b) Upper bound on the BER for codes with depolarizing rate 9.92% and encoding-rate $1/8$ as a function of system size. The probability of error decreases strongly with code size. Both the symmetric decoder and the branching-MERA improve beyond the standard quantum polar code.

that the threshold approaches the capacity with increasing code size (although, much like is observed for the classical polar code, this approach is relatively slow), and that both the improved symmetric decoder and branching-MERA code have a sharper transition at equal block size. Thus, both of these improve what is the main drawback of polar codes, which is their important finite-size effects.

In Fig. 4(b) we study the performance as a function of code size. These results are a simple upper bound on the error rate achieved by summing the individual error rates of the data channels (both quadratures) and the frozen channels (the nonfrozen quadrature) that were generated in the channel-selection phase. We observe in all cases that the block-error rate decreases rapidly with the number of layers used in the codes. For classical polar codes it is known that the error rate scales as $\exp(-\sqrt{n})$; however, we would require more computational resources to study this scaling here.

Finally, our numerical results provide additional evidence that entanglement assistance is unnecessary for achieving good performance with quantum polar codes (or the branching-MERA code). Entanglement assistance was proposed [15,16] to address possible channels that exhibit poor performance in both quadratures. Fortunately, channel polarization ensures that performance is good in either or both quadratures, and further we observe that polarization improves rapidly with code size. We make this more precise in the Supplemental Material [23].

Conclusion.—In summary, we have found that TNs provide a powerful description of QEC codes and decoding algorithms, leading us to suggest new encoding and decoding techniques beyond the standard polar code. We observe that these achieve very low error rates at high data rates (approaching the coherent information rate), especially for large code sizes. The encoding and decoding procedures follow closely their classical counterparts (by

treating each quadrature in succession), and the code performance provides additional evidence that polar codes require no preshared entanglement.

This research is funded by Canada's NSERC and FQRNT through the network INTRIQ, as well as TOQATA (Spanish Grant No. PHY008-00784), the EU IP SIQS, and the MPI-ICFO Collaboration. Numerical resources were provided by Compute Canada and Calcul Québec.

[1] M.-H. Hsieh and F. Le Gall, Phys. Rev. A **83**, 052331 (2011).
[2] P. Iyer and D. Poulin, arXiv:1310.3235.
[3] D. Poulin, Phys. Rev. A **74**, 052333 (2006).
[4] E. Pelchat and D. Poulin, IEEE Trans. Inf. Theory **59**, 3915 (2013).
[5] D. Poulin, J.-P. Tillich, and H. Ollivier, IEEE Trans. Inf. Theory **55**, 2776 (2009).
[6] G. Duclos-Cianci and D. Poulin, Phys. Rev. Lett. **104**, 050504 (2010).
[7] G. Vidal, Phys. Rev. Lett. **91**, 147902 (2003).
[8] F. Verstraete and J. I. Cirac, arXiv:cond-mat/0407066.
[9] G. Vidal, Phys. Rev. Lett. **99**, 220405 (2007).
[10] I. L. Markov and Y. Shi, SIAM J. Comput. **38**, 963 (2008).
[11] Y.-Y. Shi, L.-M. Duan, and G. Vidal, Phys. Rev. A **74**, 022320 (2006).
[12] G. Evenbly and G. Vidal, Phys. Rev. Lett. **112**, 240502 (2014).
[13] Z.-C. Gu, M. Levin, and X.-G. Wen, Phys. Rev. B **78**, 205116 (2008).
[14] M. Wilde and S. Guha, IEEE Trans. Inf. Theory **59**, 1175 (2013).
[15] J. M. Renes, F. Dupuis, and R. Renner, Phys. Rev. Lett. **109**, 050504 (2012).
[16] M. M. Wilde and S. Guha, IEEE Trans. Inf. Theory **59**, 4718 (2013).
[17] J. M. Renes and M. M. Wilde, IEEE Trans. Inf. Theory **60**, 3090 (2014).
[18] M. M. Wilde, O. Landon-Cardinal, and P. Hayden, *8th Conference on the Theory of Quantum Computation, Communication and Cryptography* (Schloss Dagstuhl–Leibniz-Zentrum fuer Informatik, Dagstuhl, Germany, 2013), p. 157.
[19] J. M. Renes, D. Sutter, F. Dupuis, and R. Renner, arXiv:1307.1136.
[20] Z. Dutton, S. Guha, and M. M. Wilde, in *Proceedings of the 50th Annual Allerton Conference on Communication, Control, and Computing, Monticello, 2012* (IEEE, New York, 2012), p. 572.
[21] G. Evenbly and G. Vidal, arXiv:1307.0831.
[22] A. J. Ferris and D. Poulin, arXiv:1312.4575.
[23] See Supplemental Material at http://link.aps.org/supplemental/10.1103/PhysRevLett.113.030501 for further details regarding the general TN decoding scheme and detailed numerical results. Includes Refs. [40,41].
[24] H. F. Chau, Phys. Rev. A **58**, 905 (1998).
[25] H. Ollivier and J.-P. Tillich, Phys. Rev. Lett. **91**, 177902 (2003).
[26] R. Orus, arXiv:1306.2164.
[27] S. R. White, Phys. Rev. Lett. **69**, 2863 (1992).
[28] N. Schuch and J. I. Cirac, Phys. Rev. A **82**, 012314 (2010).
[29] P. W. Shor, in *Proceedings of the 37th Symposium on the Foundations of Computer Science* (IEEE, Los Alamitos, CA, 1996), p. 56.
[30] L. P. Kadanoff, Physics **2**, 263 (1963).
[31] L. Tagliacozzo, G. Evenbly, and G. Vidal, Phys. Rev. B **80**, 235127 (2009).
[32] A. J. Ferris, Phys. Rev. B **87**, 125139 (2013).
[33] I. Pizorn, F. Verstraete, and R. M. Konik, Phys. Rev. B **88**, 195102 (2013).
[34] A. Y. Kitaev, Ann. Phys. (Amsterdam) **303**, 2 (2003).
[35] M. A. Levin and X.-G. Wen, Phys. Rev. B **71**, 045110 (2005).
[36] N. Schuch, J. Cirac, and D. Pérez-García, Ann. Phys. (Amsterdam) **325**, 2153 (2010).
[37] R. König, B. W. Reichardt, and G. Vidal, Phys. Rev. B **79**, 195123 (2009).
[38] A. J. Ferris, Phys. Rev. Lett. **113**, 010401 (2014).
[39] E. Arikan, IEEE Trans. Inf. Theory **55**, 3051 (2009).
[40] D. Poulin and Y Chung, Quantum Inf. Comput. **8**, 987 (2008).
[41] C. Wang, J. Harrington, and J. Preskill, Ann. Phys. (Amsterdam) **303**, 31 (2003).